U/Pb dating of geodic calcite: new insights on Western Europe major tectonic events and associated diagenetic fluids

Céline Pisapia, Pierre Deschamps, Anne Battani, Stéphane Buschaert, Abel Guihou, Bruno Hamelin, Jacques Brulhet

U/Pb dating of geodic calcite: new insights on Western Europe major tectonic events and associated diagenetic fluids

Céline Pisapia [1,2,*,a], Pierre Deschamps [1], Anne Battani [2,b], Stéphane Buschaert [2,c], Abel Guihou [1], Bruno Hamelin [1] & Jacques Brulhet [2]

[1] *CEREGE, Aix-Marseille Université-CNRS-IRD, Europôle Méditerranéen de l'Arbois, 13545 Aix-en-Provence, France*

[2] *Andra, 1-7 rue Jean Monnet, 92290 Châtenay Malabry, France*

*,[a] Corresponding author/Present adress:
Institut de Physique du Globe de Paris, 1 rue Jussieu, 75238 Paris Cedex 05, France
Tel : +33 (0)1 83 95 75 95 – Fax : +33 (0)1 83 95 77 05
e-mail: celine.pisapia@gmail.com

[b] Present address: IFPEN, 1-4 Av. de Bois-Préau, 92852 Rueil-Malmaison Cedex, France
[c] Present address: BRGM, 151 Bd Stalingrad, 69626 Villeurbanne, France

Abbreviated title: U-Pb dating of diagenetic events

Abstract

This study presents the first application of the U/Pb dating method to highly Pb-depleted diagenetic geodic calcites of the Jurassic formations of the Paris basin that leads to a reappraisal of the palaeohydrogeology history of this region. Composite U/Pb ages from multiple geodes, combined with $\delta^{18}O$ analyses, reveal two main phases of diagenetic fluid circulations linked with major regional tectonic events. Dogger formations recorded a first diagenetic fluid episode at 147.8 ± 3.8 Ma, i.e. at the very beginning of the emersion of the basin during the Tithonian period and 30Ma earlier than previously assumed. $\delta^{18}O$ results confirmed that most of the calcitic cement phases that closed the porosity of these formations

precipitated at the beginning of the Cretaceous period. Oxfordian formations recorded another major meteoric fluid circulation at 33.5 ± 2.8 Ma, which can be related to the initial stage of the European Cenozoic Rift System (ECRIS), implying that the porosity of the Mesozoic formations was closed sooner than previously thought, before the main ECRIS rifting phase of Oligocene age. This study shows that U/Pb dating of secondary geodic calcite offers a new powerful way for reconstructing the coupled palaeohydrological and diagenetic history of sedimentary basins.

Keywords

U/Pb dating, geodic calcites, diagenetic phases, palaeohydrology, Paris Basin, ECRIS

Determining the relative and absolute timing of fluid flow events is of critical importance for understanding the past history of sedimentary basins and their geological reservoirs, but also their role on the modification of the petrophysical properties of rocks, on the formation and migration of hydrocarbons, or their stability for potential deep geological disposal of radioactive wastes. During fluid flow events, secondary carbonates commonly precipitate to fill the porosity or voids, therefore occurring as infilling cements or spar calcites in geodic form. These secondary carbonates are thus relics of main fluid circulations during sedimentary basin evolution and/or tectonic events. Fluid history in sedimentary basins is generally reconstructed by combining petrographical and geochemical approaches (fluid inclusions thermometry, stable isotopes...) allowing identification between different diagenetic phases (e.g. Evans & Zalasiewicz 1996; Neymark *et al.* 2002; Worden *et al.* 1999). However, in most cases such approaches provide only a relative chronology of the past fluid events due to the lack of appropriate absolute dating methods. One drastic point is thus to have access to a reliable way of dating these diagenetic events to reconstruct the paleohydrogeological and tectonic history of the basins.

Although lead-lead and uranium-lead methods have been extensively used for dating silicates and accessory minerals for decades, direct dating of carbonates is less developed (Rasbury & Cole 2009). Following the first study of Moorbath *et al.* (1987), Pb/Pb dating were performed on uranium and lead-enriched (>1ppm) limestones and marbles (e.g. Babinski *et al.* 1999; Jahn & Simonson 1995). The first U/Pb dating of carbonates with lower uranium contents (100-500 ppb) was then reported by Smith *et al.* (1991) followed by studies on quaternary corals (Getty *et al.* 2001) or speleothems (Cliff *et al.* 2010; de Ruiter *et al.* 2009; Pickering *et al.* 2010; Richards *et al.* 1998; Woodhead *et al.* 2006). A first study on diagenetic calcite concretions was reported by Israelson *et al.* (1996) on U and Pb-rich calcites with one of the highest μ ratio ($\mu = {}^{238}U/{}^{204}Pb$) ever registered on carbonate samples

65 (μ = 288 000). Further studies showed the potential of the U/Pb method for directly
66 calibrating the geological timescale or constraining the diagenetic history of sedimentary
67 formations (Becker *et al.* 2002; Li *et al.* 2014; Luczaj & Goldstein 2000; Neymark *et al.*
68 2002; Rasbury *et al.* 1997). Recent advances in LA-ICP-MS have allowed investigating U/Pb
69 dating of secondary carbonates in calcite-mineralized faults characterized by low Pb content
70 (Coogan *et al.* 2016; Roberts & Walker 2016) but as a matter of fact, only few studies that
71 report U /Pb dating of Pb-depleted secondary carbonates.

72 The Paris Basin is an intracratonic basin formed during the Permian rifting that
73 affected the Cadomian-Variscan basement of Western Europe (Guillocheau *et al.* 2000). Its
74 tectonic and sedimentary history began with a major transgressive phase, induced by the
75 Pangaea fragmentation, and marked by Permian lacustrine to Jurassic carbonated platforms
76 sedimentation at the northern part of the Tethys platform. It was followed by a main
77 regressive phase with three major continentalization phases. First, at the upper Jurassic/lower
78 Cretaceous, the opening of the Bay of Biscay induced a fragmentation of the Jurassic
79 platform and the uplift of its northern Variscan border associated with continental
80 sedimentation. This regressive trend was marked by the Late Cimmerian unconformity
81 (LCU) at the Jurassic/Cretaceous limit (Guillocheau *et al.* 2000). Then, the upper Cretaceous
82 compressional tectonics (Africa-European convergence) induced an enhanced
83 continentalization with an evolution from marine distal formations to continental depositional
84 environments. It was accompanied by erosion processes, and increased uplift of the Variscan
85 borders. The continentalization is then definitive at the upper Oligocene. Cenozoic
86 formations were thus mainly influenced by the N-S compression of the Pyrenean phase of
87 late Eocene age (40Ma) followed by E-W extension during the European Cenozoic RIft
88 System event (ECRIS) (Dèzes *et al.* 2004; Guillocheau *et al.* 2000). The ECRIS event
89 developed as passive rifting in the foreland of the Alps and the Pyrénées. It induced the

90 formation of the main grabens in Western Europe (e.g. Upper and Lower Rhine, Limagne,
91 Bresse and Eger grabens) from the North Sea to the Mediterranean sea over more than 1000
92 km and is strongly recorded in the eastern part of the Paris Basin (Dèzes *et al.* 2004). All
93 these extensional events induced a major fracturation network of the Mesozoic formations
94 allowing meteoric fluids to percolate, and the precipitation of secondary carbonated phases.
95 ECRIS is commonly described to begin at the late Eocene, by reactivation of Variscan,
96 Permo-carboniferous and Mesozoic faults, with a main extensional episode during the
97 Oligocene period (Dèzes *et al.* 2004; Schumacher 2002). The exact chronology of this
98 extensional tectonics is not precisely known but it is generally described to be younger than
99 the Priabonian P16 zone (35.2-34 Ma) (Berggren *et al.* 1985; Guillocheau *et al.* 2000).
100 Nevertheless, evidences of shallow depressions in the Upper Rhine or Bresse grabens with
101 fluvio-lacustrine sediments might be attributed to an initial rifting phase at the middle Eocene
102 period (Dèzes *et al.* 2004; Sissingh 1998) and the debate is still open as no absolute dating
103 constraints exist.

104 The main objective of this study was thus to bring for the first time absolute age
105 constraints on major tectonic events that affected Western Europe through U/Pb dating of
106 secondary diagenetic geodic calcites. A precise dating of major fluid circulation episodes
107 induced by the first emersion phase of the Paris Basin border and by the activation of the
108 European Cenozoic RIft System event (ECRIS) was thus achieved and gave new insights on
109 these major geological events that affected the European plate.

110

111 **Geological Setting**

112 The Eastern part of the Paris Basin (France) is characterized by Carboniferous to Cenozoic
113 sedimentary formations with a monocline structure slightly dipping westwards due to the
114 subsidence of the center part of the basin (Guillocheau *et al.* 2000). Oxfordian and Dogger

115 limestones embed the Callovo-Oxfordian clayrock unit (COx) that was recognized by the
116 French National Radioactive Waste Management Agency (Andra) as a favorable host rock
117 formation for radioactive waste disposal for High-Level and Intermediate-Level Long-Lived
118 Radioactive Wastes (HLW-LL and ILW-LL) (Delay *et al.* 2007). This area experienced
119 various tectonic phases from the end of the Mesozoic till the Oligocene extension tectonics
120 and the Rhine graben formation but presents limited impact of deformation (low seismicity,
121 little deformation and vertical displacement). These formations are affected by a fracturation
122 network, which is responsible for the compartments segmentation of the basin. Several
123 grabens are present at the south of the Andra Underground Research Laboratory (URL)
124 (Joinville, Gondrecourt and Neufchateau graben) as witnesses of the Oligocene extensional
125 tectonics (Fig. 1). The sedimentary sequence was investigated by a deep borehole drilling
126 program (Delay *et al.* 2007) and presents continuous deposits from Lower Cretaceous to
127 infra-Jurassic formations.
128 The COx formation (150-160Ma) is a low-porosity detrital claystone cemented by 25-30
129 wt% of microcrystalline calcite. Its diagenetic history occurred quite early in a marine
130 environment since no major modification was noticed after. Furthermore, the calcite cements
131 of this formation present $\delta^{18}O$ values typical of unmodified marine calcite indicating that the
132 COx has not been affected by further fluid circulations (Buschaert *et al.* 2004).
133 The diagenetic history of the embedding Oxfordian and Dogger limestones is more complex.
134 These formations are affected by several generations of stratiform stylolites and dissolution
135 veins, filled with detrital clay minerals and secondary minerals such as pyrite or dolomite
136 (Andre *et al.* 2010). Thorough examination of U-series disequilibrium within these
137 stylolitized zones has shown systematic ($^{234}U/^{238}U$) activity ratio disequilibria (Deschamps et
138 al., 2004) indicating uranium remobilization and active transfer related to these
139 pressure/dissolution structures. Nevertheless, this uranium remobilization is limited to a few

centimeters range apart from the stylolites and the whole carbonates present a ($^{234}U/^{238}U$) activity ratio at equilibrium. These embedding limestones have very low porosity (2-5%) and permeability (10^{-9} to 10^{-10} $m.s^{-1}$) (Battani *et al.* 2011). By contrast with the COx formation, they rarely show the preservation of typical structures of early marine cements (micro-crystalline cement and small euhedral crystals of micro-spar). The primary and secondary porosities, as well as macro-cavities and micro-fractures, are mainly infilled by secondary sparry calcites. The remaining inter-particle porosity is infilled by large crystals of sparite isotopically similar to those observed in macro-cavities and in fractures inherited from the Eocene-Oligocene extension (Buschaert *et al.* 2004). Successive generations of blocky calcites (Cal1, Cal2, Cal3 and Cal4) were identified by microscopic observations (Carpentier *et al.* 2014). Based on oxygen and carbon isotopic analyses, they were interpreted as precipitated from meteoric fluids with carbon of local origin (Brigaud *et al.* 2009; Buschaert *et al.* 2004; Carpentier *et al.* 2014; Vincent *et al.* 2007). This excludes an early diagenetic cementation phase by marine fluids and marks later diagenetic events. Cal1 (former BC1 from Brigaud *et al.* 2009) were then assumed to precipitate at the early Cretaceous (during LCU) following the uplift of the London-Brabant massif, Cal2 (former BC2 from Brigaud *et al.* 2009) during the Late Aptian Unconformity (LAU) that was associated with erosion and karstification of the Paris Basin borders and Cal3 to the Pyrenean compression. Finally, Cal4 (former BC3 from Brigaud *et al.* 2009) was related to the Oligocene extension tectonics with the formation of main regional grabens and associated terrestrial sedimentation (Brigaud *et al.* 2009; Carpentier *et al.* 2014). Nevertheless, no absolute geochronological constraints are available for these blocky calcites and the question is still subject to debate (Andre *et al.* 2010; Brigaud *et al.* 2009; Buschaert *et al.* 2004; Vincent *et al.* 2007). The main purpose of this study was thus to date precisely these phases of fluid circulation thanks to secondary

geodic calcites U/Pb dating in order to refine the geological history of the Paris Basin and to give new insights on the major tectonic events that affected Western Europe.

Material and Methods

Geodic calcite samples

Geodic calcites were sampled from 3 Andra boreholes (HTM102, EST205 and EST433 boreholes, Fig. 2). HTM102 core was drilled 3 km SE from the URL through upper Oxfordian to upper Bathonian formations; EST205 borehole was drilled at the URL through Kimmeridgian to Oxfordian formations and EST433 borehole was drilled 8km NNW from the URL through Kimmeridgian to Bundstandstein formations. Oxfordian calcites were sampled from HTM102 and EST205 cores and Dogger calcites from EST433 core (Table 1). Six geodes were investigated in the Oxfordian sediments from 256 m to 331 m for HTM102 (5 geodes) and at 375 m for EST205 (1 geode). 13 sub-samples were analyzed from these 6 geodes. Three geodes were investigated in the Dogger formation from 799 m to 890 m for EST433 and 9 sub-samples were analyzed. Geodic calcites were carefully sampled using clean diamond drills only devoted to this study and cleaned by successive ultrasonic baths with mQ H_2O.

Geodic samples were automorphic millimetric to centrimetric semi-translucent calcite minerals with no oxidation traces. The selected geodes were not connected to stylolites to avoid any recent uranium remobilization (Deschamps *et al.* 2004).

Chemical preparation

Prior to sample dissolution, a ^{205}Pb-^{236}U-^{233}U-^{229}Th spike was added to each sample. The spike solution was primarily calibrated by analyzing the spike solution alone, with various amounts of a mixed solution of NBS-981 Pb and NBS-960 U standards, and in reference to

189 the nominal value of 137.88 for $^{238}U/^{235}U$ of natural uranium and to the concentrations of
190 NBS standards. Values of 0.95883 ± 0.00059 and 5.4677 ± 0.0034 pmol.g^{-1} were determined
191 for $^{205}Pb/^{233}U$ ratio and Pb concentration of the spike solution, respectively.
192 The chemical separation and purification of lead and uranium isotopes procedure were
193 adapted from Babinski *et al.* (1995) and Horwitz *et al.* (1992), respectively. Calcites samples
194 ranging from 140 mg to 400 mg were dissolved with a slight stoichiometric excess of 0.6N
195 HBr. Samples were directly loaded on previously cleaned AG1X8 resin (100-200 mesh, 200
196 μL) converted into HBr form with 0.6N HBr. Both sample loading and rinsing steps were
197 recovered and kept for uranium purification. Pb fraction was eluted by 6N HCl and was
198 evaporated to dryness at 120°C. Two successive purification steps of Pb samples were
199 performed after loading on AG1X8 (50 μL) and elution with 6N HCl. Taking into account
200 the very low lead concentrations of the samples, the recovery yield of this protocol was
201 carefully optimized to obtain nearly 100 %.
202 Uranium fractions were recovered after co-precipitation with iron hydroxide, dissolution with
203 4N HNO_3 and loading on previously cleaned UTEVA resin converted into nitric form with
204 4N HNO_3. Uranium samples were eluted with mQ H_2O and evaporated to dryness (120°C). A
205 purification step was performed on UTEVA resin following the same protocol.
206 Final uranium and lead samples were evaporated to dryness with one H_3PO_4 drop.
207 Similar procedures without calcite samples were conducted for lead and uranium blanks
208 determination (concentration and isotopic composition).
209
210 ***U and Pb isotopic analyses***
211 Uranium and lead isotopic compositions were determined by Thermal Ionization Mass
212 Spectrometry (VG sector-54). Lead samples (from 0.7 to 9.2 ng) were prepared with 2.8 μL
213 of silica gel and loaded on pre-degassed rhenium monofilaments. Uranium samples (from 6.5

214 to 307.2 ng) were dissolved with 1µL HNO_3 0.05N and were loaded on individual pre-
215 degassed rhenium monofilaments between two graphite lays.
216 Uranium isotopes signals (^{233}U, ^{234}U, ^{235}U, ^{236}U, ^{238}U) and lead isotopes signals (^{204}Pb, ^{205}Pb,
217 ^{206}Pb, ^{207}Pb and ^{208}Pb) were measured on a Daly ion counter with a 20 ns and 22 ns dead-time
218 value, respectively. Data considered in this study formed a linear array in both $^{207}Pb/^{206}Pb$ vs.
219 $^{204}Pb/^{206}Pb$ and $^{208}Pb/^{206}Pb$ vs. $^{204}Pb/^{206}Pb$ diagrams and were aligned for both Oxfordian and
220 Dogger samples (Fig. S1). Replicates of NBS SRM-981 standard gave an external
221 reproducibility of 0.5 ‰ for $^{208}Pb/^{206}Pb$ ratio (2.1636 ± 0.012) and of 2.9 ‰ on $^{204}Pb/^{206}Pb$
222 ratio (0.059292 ± 0.00018). Replicates of NBS SRM-960 standard gave an external
223 reproducibility of 1.5 ‰ on $^{235}U/^{234}U$ ratio (136.8892 ± 0.1993). The uranium ($^{234}U/^{238}U$)
224 activity ratio was calculated using the decay constants $\lambda^{234}U = 2.8263\ 10^{-6}$ (Cheng *et al.*
225 2000) and $\lambda^{238}U = 1.5513\ 10^{-10}$ (Jaffey *et al.* 1971) and was checked to be at equilibrium for
226 the samples considered in this study.
227 Uranium and lead blank concentrations and isotopic compositions were determined for each
228 analytical series. Uranium blanks were very good around 10 pg (10 ± 3 pg, n = 4) for all
229 analytical sessions except for the first session (187 pg). These values were similar and in the
230 lower range of published data in similar conditions (Getty & de Paolo 1995; Grandia *et al.*
231 2000; Israelson *et al.* 1996; Pickering *et al.* 2010; Smith *et al.* 1991). Lead blanks obtained all
232 along analytical sessions (117 ± 37 pg, n = 5) were in the range of published data on similar
233 size (100 to 400 mg) calcite samples (Becker *et al.* 2002; Cliff *et al.* 2010; Getty & de Paolo
234 1995; Israelson *et al.* 1996; Pickering *et al.* 2010; Polyak *et al.* 2008; Richards *et al.* 1998;
235 Smith *et al.* 1991). Nevertheless, the analyzed Pb amounts (from 0.8 ng to 8.1 ng for
236 Oxfordian samples and from 1.2 ng to 5.1 ng for Dogger samples) were in the lower range of
237 published data on continental carbonates (Cliff *et al.* 2010; de Ruiter *et al.* 2009; Getty *et al.*
238 2001; Pickering *et al.* 2010; Richards *et al.* 1998). Consequently, Pb blanks from chemical

239 procedures were not negligible and corresponded to 4 ± 3% in average of the sample Pb
240 content and up to 15 % for samples with the lowest Pb content, which can significantly
241 contribute to total final error of data. Isotopic raw data were then treated according to the
242 data-reduction technique proposed by Schmitz & Schoene (2007). Each sample was corrected
243 from the isotopic composition and concentration of the associated blank sample prepared and
244 analyzed during the same analytical session, and with an additional error corresponding to the
245 standard error of all the Pb blank concentrations. The accuracy of this correction and
246 influence on age calculation were checked by comparing results obtained from data before
247 and after blank corrections (Fig. S2 and Table S1).
248 U/Pb isochrons were constructed using Isoplot software 3.0. from Ludwig (2003).
249 Considering that analyzed calcites came from different samples precipitated from fluids with
250 possible different initial lead isotopic composition, model 2 and 3 solutions from Isoplot
251 software were used to calculate ages.
252
253 ***$\delta^{18}O$ and $\delta^{13}C$ analyses***
254 Stable isotopic analyses ($\delta^{18}O$ and $\delta^{13}C$) were conducted on crushed geodic calcite samples
255 using a mass spectrometer (Finnigan Delta Advantage) equipped with a carbonate device.
256 Measured isotopic values were normalized against international standard NBS-19. Mean
257 external reproducibility was better than 0.03 ‰ for $\delta^{13}C$ and 0.05 ‰ for $\delta^{18}O$. Each geode
258 was analyzed with 3 aliquots of 60μg weight each.
259
260 **Results**
261
262 ***U and Pb isotopic compositions of geodic calcites***
263 Results obtained on calcites from geodes are summarized Table 1.

All geodic calcites considered for this study presented very low concentration of Pb, ranging from 3.4 to 21.7 ppb and from 4.2 to 17.5 ppb for Oxfordian and Dogger samples, respectively. They also presented relatively low radiogenic ^{206}Pb signals with $^{206}Pb/^{204}Pb$ ratio from 23.1 ± 0.3 to 95.6 ± 18.8 for Oxfordian geodes and from 26.0 ± 0.3 to 110.8 ± 4.1 for Dogger geodes.

Samples presented more variable concentrations of U (from 43.8 to 782.4 ppb and from 22.2 to 331.8 ppb for Oxfordian and Dogger geodes, respectively) with μ ratios ($^{238}U/^{204}Pb$) from 256.3 ± 4.2 to 13258.6 ± 2849.6 and from 243.5 ± 1.8 to 3916.4 ± 155.6 for Oxfordian and Dogger geodes, respectively (Table 1).

Oxfordian and Dogger samples were then used for isochron reconstructions with Isoplot 3.0 software (Ludwig 2003). In both cases, absolute dating was achieved from composite isochrons obtained from several sub-samples from different geodes sampled at different depths and from several drill cores. The calculated ages are then likely to represent regional fluid flow episodes. Two distinct patterns were observed for Oxfordian and Dogger samples. Data were plotted on Tera-Wasserburg diagrams (Fig. 3) and gave an age of 33.5 ± 2.8 Ma for the Oxfordian samples (MSWD = 23, model 2 solution, 95% confidence) and of 147.8 ± 3.8 Ma (MSWD = 41, model 2 solution, 95% confidence) for the Dogger samples. Considering the limited size of each geode, sub-sampling was not sufficient to achieve a complete dating of each geode. It was only possible to determine an isochron age for a single geode (G10) from the Dogger formation. The 6 sub-samples of this geode exhibited an age of 144.6 ± 9.2 Ma (MSWD = 27, model 2 solution, 95% confidence) on a Tera-Wasserburg diagram and of 145.2 ± 8.9 Ma (MSWD = 32, model 3 solution, 95% confidence) on a ^{238}U-^{206}Pb plot (Fig. 4). These results were consistent with the calculated ages from the global composite isochrons obtained for Dogger samples (Figs. 3b and S3b,d).

The initial lead isotopic compositions were calculated to be 20.7 ± 2.2 for $^{206}Pb/^{204}Pb$ and 15.8 ± 0.2 for $^{207}Pb/^{204}Pb$ for the Oxfordian geodes and of 20.4 ± 1.2 for $^{206}Pb/^{204}Pb$ and 15.8 ± 0.1 for $^{207}Pb/^{204}Pb$ for the Dogger geodes, thus indistinguishable from each other.

Geodic calcites $\delta^{18}O$ and $\delta^{13}C$ composition

Results from stable isotopes are summarized Table 2 and Fig. 5 for all geodes. They were reproducible from one aliquot to another for each geode and between different analytical sessions. The $\delta^{18}O$ and $\delta^{13}C$ data (Fig. 5) were in agreement and within the range of previous published data on spar cements, vugs or fracture infillings of Mesozoic carbonated formations of the Eastern part of the Paris Basin (Andre *et al.* 2010; Brigaud *et al.* 2009; Buschaert *et al.* 2004; Carpentier *et al.* 2014; Vincent *et al.* 2007). Similarly to U/Pb dating, two patterns were observed between Oxfordian and Dogger samples. All geodes from Oxfordian sediments (G1 to G6) presented the same $\delta^{18}O$ range values between -10.24 ‰$_{PDB}$ and -8.95 ‰$_{PDB}$ (mean $\delta^{18}O_{PDB}$ = -9.28 ± 0.46 ‰) and $\delta^{13}C$ values between +2.22 ‰$_{PDB}$ and +2.70 ‰$_{PDB}$ (mean $\delta^{13}C_{PDB}$ = +2.5 ± 0.2 ‰). These data fell into the range of the previously described Cal4 blocky calcite (Fig. 5). Similarly, all geodes from Dogger samples (G8 to G10) had the same $\delta^{18}O$ range values between -6.72 ‰$_{PDB}$ and -6.42 ‰$_{PDB}$ (mean $\delta^{18}O_{PDB}$ = -6.54 ± 0.15 ‰) and $\delta^{13}C$ values between +1.92 ‰$_{PDB}$ and +2.49 ‰$_{PDB}$ (mean $\delta^{13}C_{PDB}$ = +2.2 ± 0.3‰) corresponding to the Cal2 blocky calcite range (Fig. 5).

Discussion

U/Pb dating of Pb-depleted geodic calcites

To our knowledge, this is the first time that U-Pb dating was made directly on highly Pb-depleted diagenetic geodic calcite samples for paleohydrogeology reconstructions in a sedimentary basin. As mentioned by Rasbury and Cole (2009), U-Pb dating of carbonate

samples require a particular attention during the analytical steps (choice of sample, chemical procedure and blanks contribution, isotopic analyses). The main bias when dating Pb-depleted carbonates samples resides in the chemical procedure and blanks correction. As explained before, our data were then carefully corrected from Pb blanks using the data-reduction technique from Schmitz & Schoene (2007).

Isochron reconstructions gave MSWD higher than 1 in all cases (Fig. 3). We have thus to consider our results as errochrons, which is commonly observed for carbonate samples (e.g. de Ruiter *et al.* 2009; Getty *et al.* 2001; Pickering *et al.* 2010; Rasbury & Cole 2009). Part of this high MSWD might be explained by analytical errors. Notably internal errors on our data were very low, inducing small error ellipses and artificially increasing MSWD values as previously evoked by Cole *et al.* (2005). This point was confirmed by the small MSWD obtained on ^{235}U-^{207}Pb plots (0.15 and 0.56 for Oxfordian and Dogger samples, respectively, Fig. S3) with larger analytical errors and error ellipses. Similarly, it is confirmed by the strong influence of Pb blank correction and error propagations on MSWD values (Table S1). We observed a great decrease of MSWD values after age calculations from data corrected from Pb blanks relative to calculations from data not corrected from Pb blanks, whereas no influence was observed on calculated ages. But, the high MSWD obtained from the Terra-Wasserburg plots might not be totally explained by analytical errors. This high scatter of the isochron data may be induced by (i) variation in the initial disequilibrium (mainly $^{234}U/^{238}U$) between the intermediate daughters of uranium series, (ii) open-system conditions with gain or loss of intermediate compounds or (iii) heterogeneity of initial Pb isotopic composition (Cole *et al.* 2005). This last point was also evoked by Rasbury & Cole (2009) who have shown that slight variations of the initial lead isotopic compositions may induce non-negligible MSWD variations. In this study, the great concordance of the calculated ages for ^{238}U and ^{235}U decay series and Tera-Wasserburg Concordia (34.6 ± 3.1 Ma, 29.7 ± 9.2 Ma

and 33.5 ± 2.8 Ma, respectively for Oxfordian samples and 147.1 ± 3.5 Ma, 152.8 ± 7.7 Ma and 147.8 ± 3.8 Ma, respectively for Dogger samples, Figs. 3 and S1) advocates for a minimal influence of $^{234}U/^{238}U$ disequilibria and allows to rule out any secondary opening of the system (Cole *et al.* 2005). At the contrary, age calculations were done from composite isochrons using geodic calcites sampled at different depths and from different cores a few kilometers away in the basin (Figs. 1 and 2). They are representative of fluid flow events at a regional scale. Geodes used for these calculations may then have been precipitated from fluids with slight fluctuations of the initial lead isotopic composition. These latter, inherent to natural carbonated environments, were similarly often assumed to be responsible for quite large MSWD of calculated isochrons (de Ruiter *et al.* 2009; Getty *et al.* 2001; Pickering *et al.* 2010). Moreover, we cannot also rule out that part of the scatter around the isochron lines reflected in high MSWD is tied to the duration of the precipitation of calcite in vugs. Inherent to the use of U/Pb isochrons is that formation of the analyzed phase is instantaneous. This assumption is very likely no longer valid when the method is applied to geodic calcites that witness to processes such as fluid circulations and porosity sealing which might have occurred during time-laps of a few million years. Consequently, in this study, high MSWD might then reflect geological processes such as heterogeneity of natural fluids or duration of diagenetic events as well as low data internal errors. For these reasons, we can reasonably consider that the calculated ages reflect major geological events occurring at a regional scale in the investigated area.

Paleofluids circulations and major related tectonic events.

Fluids composition and origin

The stable isotopic composition in oxygen and carbon of the analyzed geodes indicated two patterns in agreement with previous published data (Andre *et al.* 2010; Brigaud

363 *et al.* 2009; Buschaert *et al.* 2004; Carpentier *et al.* 2014; Vincent *et al.* 2007). Indeed, except
364 Vincent *et al.* (2007) who obtained a -9 ‰ $\delta^{18}O_{/PDB}$ value for all spar cements, Brigaud *et al.*
365 (2009), Buschaert *et al.* (2004) and Carpentier *et al.* (2014) reported a wider range for $\delta^{18}O$
366 values of spar cements and vugs in both Oxfordian and Dogger formations. The different
367 identified blocky calcites presented distinct $\delta^{18}O_{/PDB}$ values while their $\delta^{13}C_{/PDB}$ were similar
368 (see Fig. 5). All geodes from Oxfordian formations presented the same range of $\delta^{18}O$ and
369 $\delta^{13}C$ values than Cal4 blocky calcites. Similarly, all geodes from Dogger samples presented
370 $\delta^{18}O$ and $\delta^{13}C$ data related to Cal2 blocky calcites.

371 As previously mentioned by Buschaert *et al.* (2004), the $\delta^{13}C$ values of the blocky
372 calcites directly reflect and vary with the ones of the host limestones indicating a local origin
373 of the carbon. Similarly, the $\delta^{13}C$ values of geodic calcites obtained in this study (Fig. 5)
374 were similar for both Oxfordian and Dogger samples, and consistent with those of the
375 limestones (from 2.04 ‰ to 3.39 ‰) implying a similar local source of the carbon. Based on
376 $\delta^{18}O$ data and microthermometry calculations from primary fluid inclusions analyses,
377 Brigaud *et al.* (2009), Buschaert *et al.* (2004), Carpentier *et al.* (2014) and Vincent *et al.*
378 (2007) also demonstrated that the blocky calcites, jointly with calcites from vugs and macro-
379 cavities, were precipitated from the input of fresh meteoric waters. These fluids may have
380 circulated thanks to the direct connection of the limestone aquifers with surface water or to
381 the circulation of water through regional fault system (Buschaert *et al.* 2004). Similarly, $\delta^{18}O$
382 values of geodic calcites were consistent with those of blocky calcites. It highly suggested
383 that geodes might also have been precipitated from meteoric water without any seawater
384 mixing. This tends to confirm that the fluids that precipitated all geodes were of local
385 meteoric origin.

386

387 *Paleohydrological history of the eastern part of the Paris Basin*

Two major events were clearly identified from both U/Pb and stable isotopic data of geodic calcites. Considering that analyzed geodes for both Oxfordian and Dogger formations came from different cores and at different depth, we may consider that these two events were related to major phases of fluid circulations and then to regional tectonic events. We can then replace these two events into the tectonic and diagenetic history of the sedimentary basin.

The first phase of fluid circulation occurred at 147.8 ± 3.8 Ma and deeply affected the Dogger formations, as determined thanks to global composite isochron (Fig. 3) and to individual geode age calculation (Fig. 4). These geodes from Dogger formations clearly presented the same $\delta^{18}O_{/PDB}$ range (-6.5 ± 0.2 ‰) than blocky calcites Cal2. We then assume that both analyzed geodes and Cal2 were synchronous in Dogger formations. As the blocky calcites (Cal1 to Cal4) were supposed to be witnesses of major phases of fluid circulations, Brigaud *et al.* (2009) and Carpentier *et al.* (2014) correlated these diagenetic phases to major regional tectonic events and emersion phases. They assumed that Cal1 precipitated during the Late Cimmerian Unconformity (LCU) during early Cretaceous, which is commonly associated to a widespread erosional event in western Europe and to the uplift of the London-Brabant massif and of the Paris Basin borders (Guillocheau *et al.* 2000). They also postulated that Cal2 precipitated later during the Late Aptian Unconformity (LAU) at the Albian/Aptian transition (≈113 Ma) that induced a major erosion episode with karstification and ferricrete soil formation. However according to our absolute U/Pb dating of geodes from the Dogger formations at 147.8 ± 3.8 Ma, all the secondary mineral precipitations from Cal1 to Cal2 occurred during the Tithonian period, which means ~30Ma sooner than initially proposed by Brigaud *et al.* (2009) and Carpentier *et al.* (2014). This also means that most of the porosity of the Dogger formations was closed at the beginning of the Cretaceous period considering that Cal1 and Cal2 may represent up to 90% of total volume cement in Middle Jurassic limestones (Brigaud *et al.* 2009; Carpentier *et al.* 2014). It is usually postulated that the

413 emerged islands at the end of the Jurassic period were not sufficient to induce large meteoric
414 fluid percolations into Mesozoic formations. Nevertheless, several massif at the northern and
415 southern borders of the Paris Basin (i.e. Rhenish, Bohemian and London Brabant massif to
416 the north and Morvan to the south) were shown to uplift as soon as the upper Jurassic linked
417 to the Late-Cimmerian phase tectonics and to the rifting and oceanic accretion of the Bay of
418 Biscay (Beccaletto *et al.* 2011; Schumacher 2002; Thiry *et al.* 2006; Vercoutere & Van den
419 Houte 1993). This induced an erosion of their Paleozoic to early Mesozoic sedimentary cover
420 between the end of the Jurassic and the late Cretaceous (Thiry *et al.* 2006; Vercoutere & Van
421 den Houte 1993). This erosion was recorded through karstifications, paleosoils and
422 paleosurfaces that were representative of a residual infra-Cretaceous relief (Quesnel 2003)
423 and were dated from 120 to 140 Ma and up to 160 Ma (Théveniaut *et al.* 2007; Thiry *et al.*
424 2006). Consequently the uplift of these massifs may have favored the emersion of Mesozoic
425 formations and then percolation of meteoric fluids. Nevertheless, if the emersion of the
426 Tithonian formations at the end of the Jurassic period was established, there is no evidence
427 for the emersion of Dogger at that time. It is mainly due to the Late Aptian Unconformity
428 that had truncated LCU and Jurassic formations (Guillocheau *et al.* 2000), but it does not
429 preclude a possible emersion of Dogger formations associated with meteoric fluid
430 percolation at that time. Our U/Pb absolute dating seems to corroborate this hypothesis, and
431 gives new information about the initiation of the infra-cretaceous unconformity at the
432 Tithonian period. It may imply marked concomitant uplift and erosion processes at that time,
433 bringing Dogger formations at the surface. These data may then indicate that a major phase
434 of meteoric fluid circulation and diagenetic precipitation could have occurred as soon as the
435 Tithonian period inducing the formation of main geodes and all blocky sparites from Cal1 to
436 Cal2 into Dogger formations, and of Cal1 and Cal2 cements in Oxfordian formations. It is
437 also consistent with the microscopic observations that both Cal1 and Cal2 infill F1 fractures

assumed to be of Kimmeridgian/Tithonian age and that mainly affected Middle Jurassic formations (Carpentier *et al.* 2014).

The second main phase of fluid circulation at 33.5 ± 2.8 Ma was solely recorded in geodic calcites from the Oxfordian formations. It was clearly related to BC3/Cal4 calcites evoked by Brigaud *et al.* (2009), Buschaert *et al.* (2004) and Carpentier *et al.* (2014) with similar mean $\delta^{18}O_{/PDB}$ values ($\delta^{18}O_{/PDB}$ = -9.3 ± 0.5 ‰, Fig. 5). Previous studies attributed BC3/Cal4 precipitation to the Eocene/Oligocene extension tectonics, during the ECRIS, considering that BC3/Cal4 $\delta^{18}O$ values were similar to the ones of the infilling calcites of Eocene/Oligocene fractures. The absolute U/Pb dating of geodic calcites at 33.5 ± 2.8 Ma is consistent with this conclusion. It is also in agreement with the U/Th-He dating attempts of fracture-infilling calcites from the ECRIS-induced fractures at the Gondrecourt graben (Cros *et al.* 2014). Due to He diffusion, U/Th-He dating gave highly variable ages (from 0.2Ma to 204Ma) that were not reproducible among 63 samples except for one sample at 29-36Ma. U/Pb dating of geodic calcites shows then accurately the existence of a main phase of meteoric fluid circulation induced by the fracturation of the carbonate formations of the eastern part of the Paris Basin during the ECRIS tectonics. This tectonic event that affected western and central Europe was activated during the late Eocene and was followed by a main rifting phase at the Oligocene. During the Late Eocene, the Alpine foreland was subjected to intra-plate compressional stresses induced by Alpine and Pyrenean collision zones (Dèzes *et al.* 2004; Ziegler 1992). These stresses reactivated late Variscan, Permo-Carboniferous and Mesozoic fracture systems that controlled the localization of the main individual grabens such as the Rhine graben in the eastern part of the Paris Basin (Schumacher 2002; Ziegler 1992). This area was marked by a widespread Bartonian phase of progressive regional uplift of the graben shoulders accompanied by meteoric fluid circulations and erosion (Sissingh, 1998). Our results indicate that large regional meteoric fluid circulations and subsequent

precipitation of secondary calcites occurred as soon as late Eocene during the initial phases of rifting. It affected all the Oxfordian formations and finally closed the porosity of the limestones. We cannot exclude that this main phase of fluid circulation could also have affected Dogger formations but to a lesser extent considering that only a few BC3/Cal4 samples were identified in Dogger rocks (Brigaud *et al.* 2009; Buschaert *et al.* 2004; Carpentier *et al.* 2014). We can also assume that the porosity of the Dogger formations was already largely closed following the late Jurassic/early Cretaceous diagenetic event. This is the first time that a reliable absolute age is given for ECRIS event. It tends to confirm that this major tectonic phase that affect all Western Europe may have begun from the Late Eocene as soon as 34Ma.

These results do not preclude the existence of phases of fluids circulations between 148Ma and 34Ma (*i.e.* during the LAU). But we can assume that these potential events, if they occurred, should have been limited by the closure of the porosity of the formations at 148Ma and might not have induced major dissolution/reprecipitation of secondary geodic calcites in the carbonated formations of the Eastern part of the Paris Basin.

Conclusion

This study presents and discusses the first U/Pb dating of diagenetic geodic calcites, highly depleted in lead, of the Mesozoic formations of the eastern part of the Paris Basin. We have shown that composite isochrons realized from different geodic calcites can allow determining the absolute age of main regional fluid flow events. We also showed that, when geodes are large enough, individual age of one geode can also be determined. In the present study, the obtained results on one geode were consistent with global composite isochron age. These U/Pb analyses, jointly with oxygen and carbon isotopic analyses clearly indicated two main phases of fluid circulation: at 148 Ma and 34 Ma. We have correlated these two phases

of fluid circulation and precipitation of calcite to the blocky calcite phases previously described in the literature. The absolute chronology obtained for the two major diagenetic events allow us to revisit the history of the eastern part of the Paris Basin and to demonstrate that the first phases of diagenetic closure of the porosity may have occurred sooner than previously thought. In Dogger formations, most of the spar cements were precipitated earlier than 148Ma. Nevertheless, a more recent major phase of fluid circulation occurred at 34Ma linked with the major ECRIS extension tectonics of the Eocene/Oligocene period that affected Western Europe. These results tend to indicate that meteoric fluid percolation induced by the ECRIS tectonics were important from its first stages during late Eocene, sooner than previously thought.

The U/Pb dating method of secondary calcites may then be a powerful tool for diagenetic, paleohydrological and tectonic reconstructions. This study opens new perspectives for diagenetic minerals dating and especially for future cement analyses or fault-formed carbonates.

Acknowledgements and fundings

This project was supported by Andra (French National Radioactive Waste Management Agency) and by CNRS INSU. The authors want to thank Jean David and the GEOTOP geochronology team (Montreal, Canada) for providing ^{205}Pb spike, Laurence Vidal and Corinne Sonzogni from CEREGE (Aix-Marseille Université, France) for $\delta^{18}O$ and $\delta^{13}C$ analyses, M. Cathelineau and T. Blaise from G2R UMR 7566 (Nancy Université, France) for samples, A. Trouiller (Andra), J. Delmas and P. Houel (IFPEN) for precious comments on the manuscript.

Conflict of interest statement

The authors declare no conflict of interest.

Author contribution

C. Pisapia made the analyses, data treatment and interpretation, and wrote the paper. P. Deschamps, A. Guihou, B. Hamelin participated to sample analyses and/or data treatment. All co-authors discussed the results and co-wrote the paper.

521 **References**
522
523 Andre, G., Hibsch, C. *et al.* 2010. Chronology of fracture sealing under a meteoric fluid
524 environment: Microtectonic and isotopic evidence of major Cainozoic events in the
525 eastern Paris Basin (France). *Tectonophysics,* **490**, 214–228.
526 doi:10.1016/j.tecto.2010.05.016
527 Babinski, M., Chemale, F. & Van Schmus, E.R. 1995. The Pb/Pb age of the Minas
528 Supergroup carbonate rocks, Quadrilátero Ferrífero, Brazil. *Precambrian Res.,* **72**, 235–
529 245. doi:http://dx.doi.org/10.1016/0301-9268(94)00091-5
530 Babinski, M., Van Schmus, W.R. & Chemale, F. 1999. Pb-Pb dating and Pb isotope
531 geochemistry of Neoproterozoic carbonate rocks from the Sao Francisco basin, Brazil:
532 Implications for the mobility of Pb isotopes during tectonism and metamorphism. *Chem.*
533 *Geol.,* **160**, 175–199. doi:10.1016/S0009-2541(99)00067-4
534 Battani, A., Smith, T. *et al.* 2011. Contribution of logging tools to understanding helium
535 porewater data across the Mesozoic sequence of the East of the Paris Basin. *Geochim.*
536 *Cosmochim. Acta,* **75**, 7566–7584. doi:10.1016/j.gca.2011.09.032
537 Beccaletto, L., Hanot, F., Serrano, O. & Marc, S. 2011. Overview of the subsurface structural
538 pattern of the Paris Basin (France): Insights from the reprocessing and interpretation of
539 regional seismic lines. *Mar. Pet. Geol.,* **28**, 861–879,
540 doi:10.1016/j.marpetgeo.2010.11.006
541 Becker, M.L., Rasbury, E.T., Meyers, W.J. & Hanson, G.N. 2002. U–Pb calcite age of the
542 Late Permian Castile Formation, Delaware Basin: a constraint on the age of the
543 Permian–Triassic boundary (?). *Earth Planet. Sci. Lett.,* **203**, 681–689.
544 doi:10.1016/S0012-821X(02)00877-4
545 Berggren, W.A., Kent, D. V, Swisher, C.C. & Aubry, M. 1985. A revised Cenozoic
546 geochronology and chronostratigraphy. *SEPM*, **54**, 129-212.
547 Brigaud, B., Durlet, C. *et al.* 2009. The origin and timing of multiphase cementation in
548 carbonates: Impact of regional scale geodynamic events on the Middle Jurassic
549 Limestones diagenesis (Paris Basin, France). *Sediment. Geol.,* **222**, 161–180.
550 doi:10.1016/j.sedgeo.2009.09.002
551 Buschaert, S., Fourcade, S. *et al.* 2004. Widespread cementation induced by inflow of
552 continental water in the eastern part of the Paris basin: O and C isotopic study of
553 carbonate cements. *Appl. Geochemistry,* **19**, 1201–1215.
554 doi:10.1016/j.apgeochem.2003.01.001
555 Carpentier, C., Brigaud, B. *et al.* 2014. Impact of basin burial and exhumation on Jurassic
556 carbonates diagenesis on both sides of a thick clay barrier (Paris Basin , NE France).
557 *Mar. Pet. Geol.,* **53**, 44–70. doi:10.1016/j.marpetgeo.2014.01.011
558 Cheng, H., Edwards, R.L. *et al.* 2000. The half-lives of uranium-234 and thorium-230. *Chem.*
559 *Geol.,* **169**, 17–33. doi:10.1016/S0009-2541(99)00157-6
560 Cliff, R.A., Spötl, C. & Mangini, A. 2010. U-Pb dating of speleothems from Spannagel Cave,
561 Austrian Alps: A high resolution comparison with U-series ages. *Quat. Geochronol.,* **5**,
562 452–458. doi:10.1016/j.quageo.2009.12.002
563 Cole, J.M., Rasbury, E.T. *et al.* 2005. Using U-Pb ages of Miocene tufa for correlation in a
564 terrestrial succession, Barstow Formation, California. *Geol. Soc. Am. Bull.,* **117**, 276.
565 doi:10.1130/B25553.1
566 Coogan, L.A., Parrish, R.R. & Roberts, N.M.W. 2016. Early hydrothermal carbon uptake by
567 the upper oceanic crust: Insight from in situ U-Pb dating. *Geology,* **44**, 147–150.
568 doi:10.1130/G37212.1
569 Cros, A., Gautheron, C. *et al.* 2014. 4He behavior in calcite filling viewed by (U-Th)/He
570 dating, 4He diffusion and crystallographic studies. *Geochim. Cosmochim. Acta,* **125**,

414–432. doi:10.1016/j.gca.2013.09.038
de Ruiter, D.J., Pickering, R. *et al.* 2009. New Australopithecus robustus fossils and associated U-Pb dates from Cooper's Cave (Gauteng, South Africa). *J. Hum. Evol.,* **56**, 497–513. doi:10.1016/j.jhevol.2009.01.009
Delay, J., Rebours, H., Vinsot, A. & Robin, P. 2007. Scientific investigation in deep wells for nuclear waste disposal studies at the Meuse/Haute Marne underground research laboratory, Northeastern France. *Phys. Chem. Earth,* **32**, 42–57. doi:10.1016/j.pce.2005.11.004
Deschamps, P., Hillaire-Marcel, C. *et al.* 2004. $^{234}U/^{238}U$ Disequilibrium along stylolitic discontinuities in deep Mesozoic limestone formations of the Eastern Paris basin: evidence for discrete uranium mobility over the last 1–2 million years. *Hydrol. Earth Syst. Sci.,* **8**, 35–46. doi:10.5194/hess-8-35-2004
Dèzes, P., Schmid, S.M. & Ziegler, P.A. 2004. Evolution of the European Cenozoic Rift System: interaction of the Alpine and Pyrenean orogens with their foreland lithosphere. *Tectonophysics,* **389**, 1–33. doi:10.1016/j.tecto.2004.06.011
Evans, J. & Zalasiewicz, J. 1996. U-Pb, Pb-Pb and Sm-Nd dating of authigenic monazite: implications for the diagenetic evolution of the Welsh Basin 144.
Getty, S.R., Asmerom, Y., Quinn, T.M. & Budd, A.F. 2001. Accelerated Pleistocene coral extinctions in the Caribbean Basin shown by uranium-lead (U-Pb) dating. *Geology,* **29**, 639–642. doi:10.1130/0091-7613(2001)029<0639:APCEIT>2.0.CO;2
Getty, S.R. & de Paolo, D.J. 1995. Quaternary geochronology using the U-Th-Pb method. *Geochim. Cosmochim. Acta,* **59**, 3267–3272. doi:10.1016/0016-7037(95)00197-8
Grandia, F., Asmerom, Y. *et al.* 2000. U–Pb dating of MVT ore-stage calcite: implications for fluid flow in a Mesozoic extensional basin from Iberian Peninsula. *J. Geochemical Explor.,* **69–70**, 377–380. doi:http://dx.doi.org/10.1016/S0375-6742(00)00030-3
Guillocheau, F., Robin, C. *et al.* 2000. Meso-Cenozoic geodynamic evolution of the Paris Basin: 3D stratigraphic constraints. *Geodin. Acta,* **13**, 189–245. doi:10.1016/S0985-3111(00)00118-2
Horwitz, E.P., Dietz, M.L. *et al.* 1992. Separation and preconcentration of uranium from acidic media by extraction chromatography. *Anal. Chim. Acta,* **266**, 25–37. doi:10.1016/0003-2670(92)85276-C
Israelson, C., Halliday, A.N. & Buchardt, B. 1996. U-Pb dating of calcite concretions from Cambrian black shales and the Phanerozoic time scale. *Earth Planet. Sci. Lett.,* **141**, 153–159. doi:darobfita
Jaffey, A.H., Flynn, K.F. *et al.* 1971. Precision measurement of half-lives and specific activities of ^{235}U and ^{238}U. *Phys. Rev. C,* **4**, 1889–1906.
Jahn, B. & Simonson, B.M. 1995. Carbonate Pb-Pb ages of the Wittenoom Formation and Carawine Dolomite, Hamersley Basin , Western Australia (with implications for their correlation with the Transvaal Dolomite of South Africa). *Precambrian Res.,* **72**, 247–261.
Li, Q., Parrish, R.R., Horstwood, M.S.A. & McArthur, J.M. 2014. U-Pb dating of cements in Mesozoic ammonites. *Chem. Geol.,* **376**, 76–83. doi:10.1016/j.chemgeo.2014.03.020
Luczaj, J.A. & Goldstein, R.H. 2000. Diagenesis of the Lower Permian Krider Member, Southwest Kansas, U.S.A.: Fluid-Inclusion, U-Pb, and Fission-Track Evidence for Reflux Dolomitization During Latest Permian Time. *J. Sediment. Res.,* **70**, 762–773. doi:10.1306/2DC40936-0E47-11D7-8643000102C1865D
Ludwig, K.R. 2003. ISOPLOT a plotting and regression program for radiogenic isotope data, Version Ex/3.00.
Moorbath, S., Taylor, P.N. *et al.* 1987. First direct radiometric dating of Archean stromatolitic limestone. *Nature,* **326**, 865–867.

621 Neymark, L.A., Amelin, Y., Paces, J.B. & Peterman, Z.E. 2002. U-Pb ages of secondary
622 silica at Yucca Mountain, Nevada: implications for the paleohydrology of the
623 unsaturated zone. *Appl. Geochemistry,* **17**, 709–734. doi:10.1016/S0883-
624 2927(02)00032-X
625 Pickering, R., Kramers, J.D. *et al.* 2010. U–Pb dating of calcite–aragonite layers in
626 speleothems from hominin sites in South Africa by MC-ICP-MS. *Quat. Geochronol.,* **5**,
627 544–558. doi:10.1016/j.quageo.2009.12.004
628 Polyak, V., Hill, C. & Asmerom Y. 2008. Age and evolution of the Grand Canyon revealed
629 by U-Pb dating of water table-type speleothems. *Science*, **319**, 1377-1380.
630 Quesnel, F. 2003. Paleoweathering and paleosurfaces from northern and eastern France to
631 Belgium and Luxembourg : geometry, dating and geodynamic implications. Géologie la
632 Fr. Spec. Conf. "Paleoweathering Paleosurf. Ardennes-Eifel Reg. (F. Quesnel coord.) 1,
633 95–104.
634 Rasbury, E.T. & Cole, J.M. 2009. Directly dating geological events: U-Pb dating of
635 carbonates. *Review of Geophysics*, **47**, 1–27. doi:10.1029/2007RG000246.1.
636 Rasbury, E.T., Hanson, G.N., Meyers, W.J. & Saller, A.H. 1997. Dating of the time of
637 sedimentation using U-Pb ages for paleosol calcite. *Geochim. Cosmochim. Acta,* **61**,
638 1525–1529. doi:darobfita
639 Richards, D.A., Bottrell, S.H. *et al.* 1998. U-Pb dating of a speleothem of Quaternary age.
640 *Geochim. Cosmochim. Acta,* **62**, 3683–3688. doi:10.1016/S0016-7037(98)00256-7
641 Roberts, N.M.W. & Walker, R.J. 2016. U-Pb geochronology of calcite-mineralized faults:
642 Absolute timing of rift-related fault events on the northeast Atlantic margin. *Geology,*
643 **44**, 531–534. doi:10.1130/G37868.1
644 Schmitz, M.D. & Schoene, B. 2007. Derivation of isotope ratios, errors, and error
645 correlations for U-Pb geochronology using 205Pb-235U-(233U)-spiked isotope dilution
646 thermal ionization mass spectrometric data. *Geochemistry, Geophys. Geosystems,* **8**, 1–
647 20. doi:10.1029/2006GC001492
648 Schumacher, M.E. 2002. Upper Rhine Graben: Role of preexisting structures during rift
649 evolution. *Tectonics,* **21**. doi:10.1029/2001TC900022
650 Sissingh, W. 1998. Comparative tertiary stratigraphy of the Rhine Graben, Bresse Graben
651 and Molasse Basin: Correlation of Alpine foreland events. *Tectonophysics,* **300**, 249–
652 284. doi:10.1016/S0040-1951(98)00243-1
653 Smith, P.E., Farquhar, R.M. & Hancock, R.G. 1991. Direct radiometric age determination of
654 carbonate diagenesis using U-Pb in secondary calcite. *Earth Planet. Sci. Lett.,* **105**, 474–
655 491.
656 Théveniaut, H., Quesnel, F., Wyns, R. & Hugues, G. 2007. Palaeomagnetic dating of the
657 “Borne de Fer” ferricrete (NE France): Lower Cretaceous continental weathering.
658 *Palaeogeogr. Palaeoclimatol. Palaeoecol.,* **253**, 271–279.
659 doi:10.1016/j.palaeo.2007.01.010
660 Thiry, M., Quesnel, F. *et al.* 2006. Continental France and Belgium during the early
661 cretaceous: Paleoweatherings and paleolandforms. *Bull. la Soc. Geol. Fr.,* **177**, 155–175.
662 doi:10.2113/gssgfbull.177.3.155
663 Vercoutere, C. & Van den Houte, P. 1993. Post-Palaeozoic cooling and uplift of the Brabant
664 Massif as revealed by apatite fission track analysis. *Geol. Mag.,* **130**, 639–646.
665 Vincent, B., Emmanuel, L., Houel, P. & Loreau, J.-P. 2007. Geodynamic control on
666 carbonate diagenesis: Petrographic and isotopic investigation of the Upper Jurassic
667 formations of the Paris Basin (France). *Sediment. Geol.,* **197**, 267–289.
668 doi:10.1016/j.sedgeo.2006.10.008
669 Woodhead, J., Hellstrom, J. *et al.* 2006. U-Pb geochronology of speleothems by MC-ICPMS.
670 *Quat. Geochronol.,* **1**, 208–221. doi:10.1016/j.quageo.2006.08.002

671 Worden, R.H., Coleman, M.L. & Matray, J.M. 1999. Basin scale evolution of formation
672 waters: a diagenetic and formation water study of the Triassic Chaunoy Formation, Paris
673 Basin. *Geochim. Cosmochim. Acta,* **63**, 2513–2528.
674 Ziegler, P.A. 1992. European Cenozoic rift system. Tectonophysics 208, 91–111.
675 doi:10.1016/0040-1951(92)90338-7
676
677

678 **Table Captions**

679 **Table 1**: ***Synthesis of U and Pb elemental and isotopic data*** *obtained on geodic calcites*

680 *from the eastern part of the Paris Basin for Oxfordian and Dogger samples.*

681 **Table 2**: ***Stable isotopic data for geodic calcites*** *analyzed in this study.* $\delta^{18}O$ *and* $\delta^{13}C$ *values*

682 *are reported for the 3 aliquotes of each geode.*

683

684 **Figure Captions**

685

686 **Figure 1**: **Simplified geological map of the studied area** with the localization of EST 205,
687 EST 433 and HTM 102 cores (modified from Buschaert *et al.* 2004).

688 **Figure 2**: **Synthetic logs of EST 205, HTM 102 and EST433 cores**. The sampling positions
689 of the analyzed geodes for Oxfordian and Dogger samples are specified and optical
690 photographs of two typical analyzed geodes (G2 and G3 from HTM 102 borehole) are given.

691 **Figure 3**: **Tera-Wasserburg Concordia diagrams** for Oxfordian (**a**) and Dogger (**b**)
692 samples using Isoplot software 3.0 (Ludwig 2003) (model 2, 95% confidence) and calculated
693 ages obtained.

694 **Figure 4: $^{206}Pb/^{204}Pb$ vs. $^{238}U/^{204}Pb$ isochron** (**a**) **and Tera-Wasserburg Concordia** (**b**)
695 obtained for 6 sub-samples of one geode (G10) using Isoplot software 3.0 (Ludwig 2003) and
696 calculated ages obtained.

697 **Figure 5**: **$\delta^{18}O$ and $\delta^{13}C$ compositions of geodic calcites** analyzed in this study. Error bars
698 are within the points. Data from Oxfordian limestones, COx claystones and Dogger
699 limestones from Buschaert *et al.* (2004) are specified ($\delta^{18}O$ data were converted from SMOW
700 to PDB thanks to the equation from Coplen et al. 1983: $\delta^{18}O_{/SMOW} = 1.03091*\delta^{18}O_{/PDB} +$
701 30.91). Grey squares summarize Blocky Calcites mean data (Cal1, Cal2, Cal3 and Cal4) from
702 Brigaud *et al.* (2009) and Carpentier *et al.* (2014).

703

Table 1

Sample name	Weight (mg)	U (ppb)	Pb (ppb)	μ ($^{238}U/^{204}Pb$) ± 2σ [%]		$^{206}Pb/^{204}Pb$ ± 2σ [%]		$^{235}U/^{204}Pb$ ± 2σ [%]		$^{207}Pb/^{204}Pb$ ± 2σ [%]		$^{238}U/^{206}Pb$ ± 2σ [%]		$^{207}Pb/^{206}Pb$ ± 2σ [%]	
Oxfordian															
G1-1	395	266.2	5.8	3935.6	4.4	39.3	3.5	28.5	4.4	16.6	4.1	100.08	1.5	0.423	3.1
G1-2	407	284.8	4.2	6947.9	7.0	56.9	6.0	50.4	7.0	17.5	6.5	122.03	1.6	0.308	5.0
G1-3	324	331.3	6.2	4769.8	3.6	44.4	2.9	34.6	3.6	16.8	3.4	107.44	1.1	0.379	2.6
G1-4	144	577.8	11.1	4910.1	6.8	48.6	5.1	35.6	5.0	17.0	4.8	100.95	1.3	0.350	3.7
G2-1	378	420.7	7.2	5379.2	4.0	47.4	3.3	39.0	4.0	17.0	3.7	113.55	1.2	0.358	2.8
G2-2	402	254.8	6.8	3050.1	3.5	35.7	2.7	22.1	3.5	16.4	3.3	85.34	1.3	0.460	2.5
G2-3	118	247.4	8.1	3516.6	5.8	43.1	4.8	25.5	5.8	16.8	5.6	81.62	1.7	0.389	4.4
G3-1	237	301.3	3.4	13258.6	21.5	95.6	19.6	96.2	21.5	19.5	19.5	138.67	2.8	0.204	14.7
G3-2	261	336.2	6.8	4512.7	4.1	46.1	3.4	32.7	4.1	16.9	3.9	97.93	1.1	0.367	3.1
G4-1	372	782.4	21.7	2856.6	1.3	35.5	0.9	20.7	1.3	16.4	1.1	80.43	0.7	0.462	0.8
G5-1	348	43.8	3.7	872.3	4.6	26.0	3.4	6.3	4.6	16.0	4.5	33.56	2.2	0.614	3.3
G5-2	251	50.9	4.4	830.5	1.9	26.3	1.4	6.0	1.9	16.0	1.9	31.62	1.0	0.608	1.3
G6-1	362	35.0	9.4	256.3	1.7	23.1	1.2	1.9	1.7	16.0	1.6	11.10	0.9	0.691	1.1
Dogger															
G8-1	246	39.0	11.6	243.5	0.7	26.1	0.5	1.8	0.7	16.1	0.7	9.33	0.4	0.615	0.5
G9-1	269	22.2	5.8	272.7	1.3	26.0	1.0	2.0	1.3	16.1	1.3	10.50	0.7	0.619	0.9
G9-2	295	25.8	4.2	474.8	1.9	31.6	1.5	3.4	1.9	16.4	1.8	15.02	0.8	0.518	1.3
G10-1	279	230.3	11.2	2398.8	1.1	76.1	1.0	17.4	1.1	18.6	1.0	31.53	0.2	0.244	0.8
G10-2	289	243.1	17.5	1297.9	0.6	51.4	0.5	9.4	0.6	17.4	0.5	25.26	0.3	0.339	0.4
G10-3	224	281.6	9.8	2626.1	1.2	82.3	1.1	19.0	1.2	18.9	1.1	31.90	0.2	0.230	0.9
G10-4	250	331.8	12.7	3916.4	4.0	110.8	3.7	28.4	4.0	20.3	3.6	35.34	0.5	0.183	2.7
G10-5	244	324.7	13.3	3328.3	3.5	96.3	3.2	24.1	3.5	19.5	3.2	34.56	0.6	0.202	2.5
G10-6	260	156.6	8.7	1938.0	4.0	64.0	3.5	14.1	4.0	17.9	3.8	30.27	0.9	0.280	3.0

Table 2

Core	Sample name		$\delta^{18}O$ (‰/PDB)	± 2σ	$\delta^{13}C$ (‰/PDB)	± 2σ
Oxfordian						
EST 205	G4	EST 07057	-8.98	0.02	2.68	0.012
			-8.90	0.04	2.70	0.03
			-8.98	0.01	2.72	0.039
HTM 102	G1	HTM 00544	-9.36	0.03	2.69	0.04
			-9.21	0.01	2.73	0.04
			-9.23	0.02	2.66	0.05
	G2	HTM 00595	-9.24	0.02	2.41	0.06
			-9.18	0.03	2.43	0.02
			-9.28	0.02	2.33	0.02
	G3	HTM 80513	-8.98	0.02	2.55	0.02
			-9.02	0.02	2.54	0.03
			-8.99	0.04	2.60	0.04
	G5	HTM 02854	-10.26	0.02	2.35	0.06
			-10.20	0.02	2.36	0.02
			-10.26	0.04	2.38	0.04
	G6c	HTM 331	-8.96	0.01	2.68	0.02
			-8.95	0.02	2.70	0.02
			-9.05	0.02	2.72	0.01
Dogger						
EST 433	G8	EST 29185	-6.67	0.04	2.28	0.03
			-6.80	0.04	2.26	0,04
			-6.69	0.02	2.25	0,01
	G9	EST 29192	-6.47	0.04	2.47	0.03
			-6.33	0.02	2.51	0.03
			-6.47	0.02	2.50	0.02
	G10	EST 30904	-6.44	0.02	1.82	0.01
			-6.56	0.02	1.92	0.02
			-6.42	0.03	1.91	0.02
	G11	EST 34826	-9.37	0.05	0.39	0,02
			-9.37	0.04	0.39	0.02
			-9.36	0.03	0.41	0.02

Figure 1

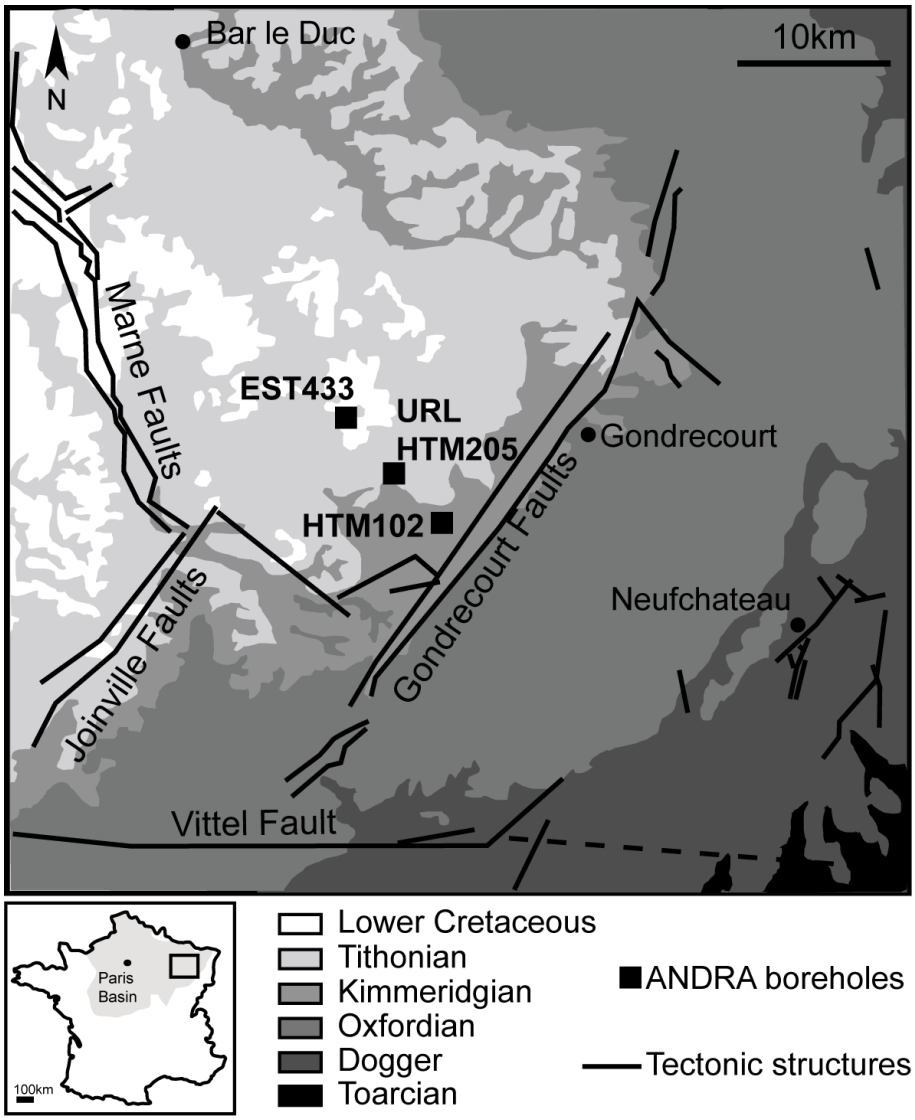

Figure 2

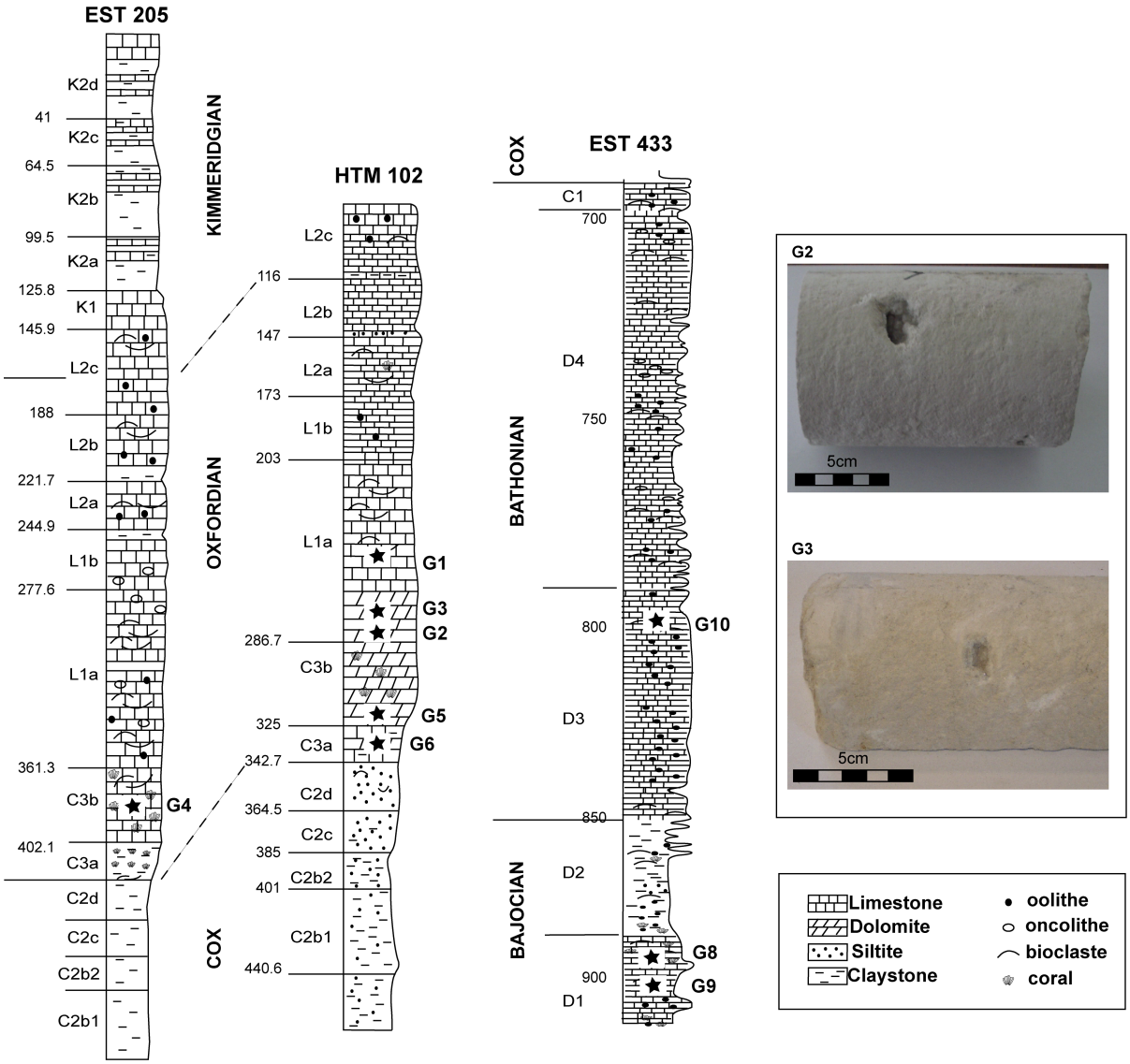
EST 205
K2d
41
K2c
64.5
K2b
99.5
K2a
125.8
K1
145.9
L2c
188
L2b
221.7
L2a
244.9
L1b
277.6
L1a
361.3
C3b
G4
402.1
C3a
C2d
C2c
C2b2
C2b1
KIMMERIDGIAN
OXFORDIAN
COX
HTM 102
116
L2c
147
L2b
173
L2a
203
L1b
L1a
G1
G3
G2
286.7
C3b
325
G5
C3a
G6
342.7
C2d
364.5
C2c
385
C2b2
401
C2b1
440.6
COX
EST 433
C1
700
D4
750
BATHONIAN
800
G10
D3
850
D2
BAJOCIAN
G8
900
G9
D1
G2
5cm
G3
5cm
Limestone
Dolomite
Siltite
Claystone
oolithe
oncolithe
bioclaste
coral

Figure 3

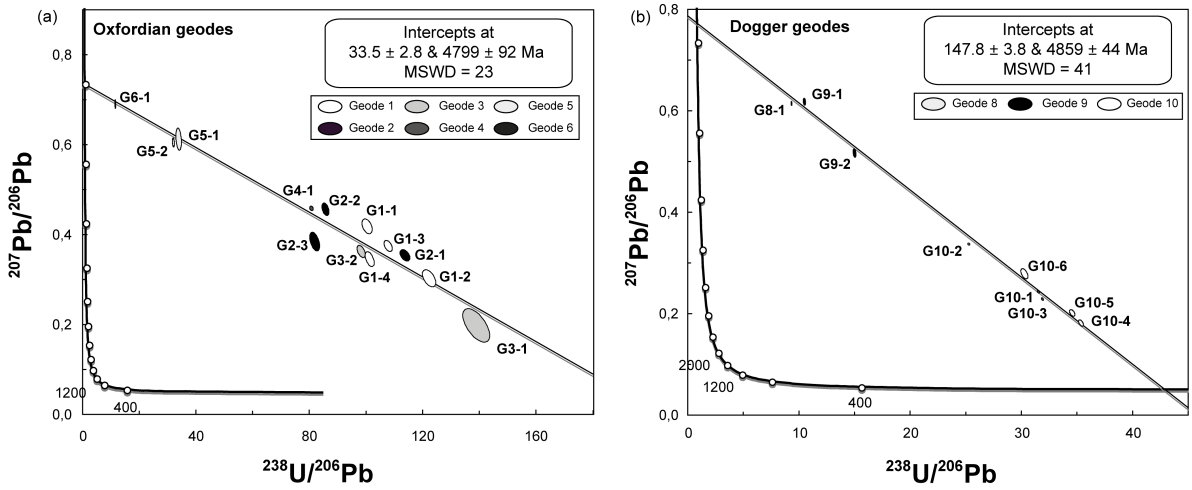

Figure 4

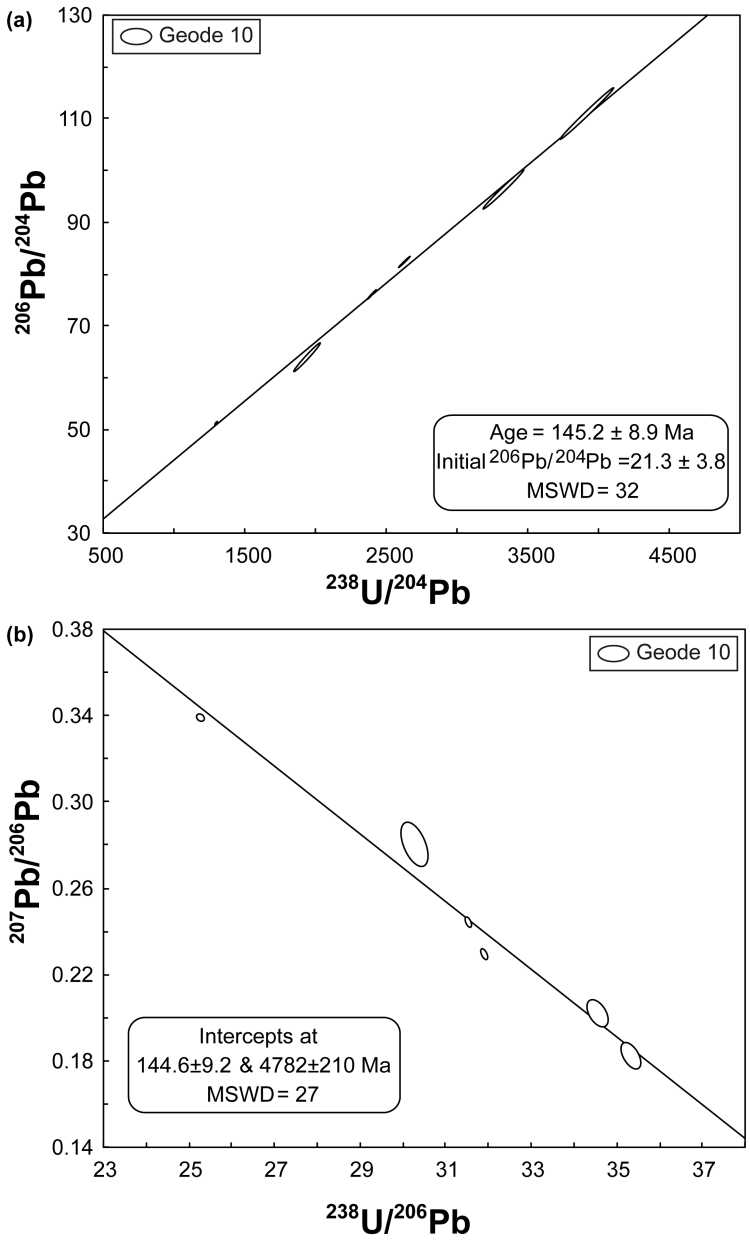

Figure 5